Electronic Supporting Information

Engineering Poly(dehydroalanine)-Based Gels via Droplet-Based Microfluidics: From Bulk to Microspheres

Hannah F. Mathews,[a,b] Tolga Çeper,[c] Tobias Speen,[a,b] Céline Bastard,[a,b] Selin Bulut,[a,b] Maria I. Pieper,[a,b] Felix H. Schacher,[c,d,e,f] Laura De Laporte,[a,b,g] and Andrij Pich*[a,b,h]

[a.] *DWI – Leibniz Institute for Interactive Materials, Forckenbeckstr. 50, 52074 Aachen (Germany). E-Mail: pich@dwi.rwth-aachen.de*
[b.] *Institute of Technical and Macromolecular Chemistry, RWTH Aachen University, Worringer Weg 2, 52074 Aachen (Germany).*
[c.] *Institute of Organic Chemistry and Macromolecular Chemistry, Friedrich-Schiller-University Jena, Humboldtstr. 10, 07743 Jena (Germany).*
[d.] *Jena Center for Soft Matter (JCSM), Friedrich-Schiller-University Jena, Philosophenweg 7, 07743 Jena (Germany).*
[e.] *Center for Energy and Environmental Chemistry Jena (CEEC), Friedrich-Schiller-University Jena, Philosophenweg 7a, 07743 Jena (Germany).*
[f.] *Cluster of Excellence Balance of the Microverse, Friedrich-Schiller-University Jena, Grüne Aue, 07754 Jena (Germany).*
[g.] *Institute of Applied Medical Engineering (AME), Department of Advanced Materials for Biomedicine (AMB), University Hospital RWTH Aachen, Center for Biohybrid Medical Systems (CMBS), Forckenbeckstr. 55, 52074 Aachen (Germany).*
[h.] *Aachen Maastricht Institute for Biobased Materials (AMIBM), Brightland Chemelot Campus, Maastricht University, 6167 RD Geleen (The Netherlands).*

Synthesis and characterisation of polydehydroalanine (PDha) macromonomer

PDha was synthesized by deprotection of P^{t}BMA with trifluoroacetic acid as already described elsewhere.[1]
^{1}H-NMR (400 Hz, D_2O/NaOD ≈ 7:3): δ (ppm) = 2.7 (s, 3H, O-CH_3), 1.69 – 1.90 (m, 2H, CH_2).

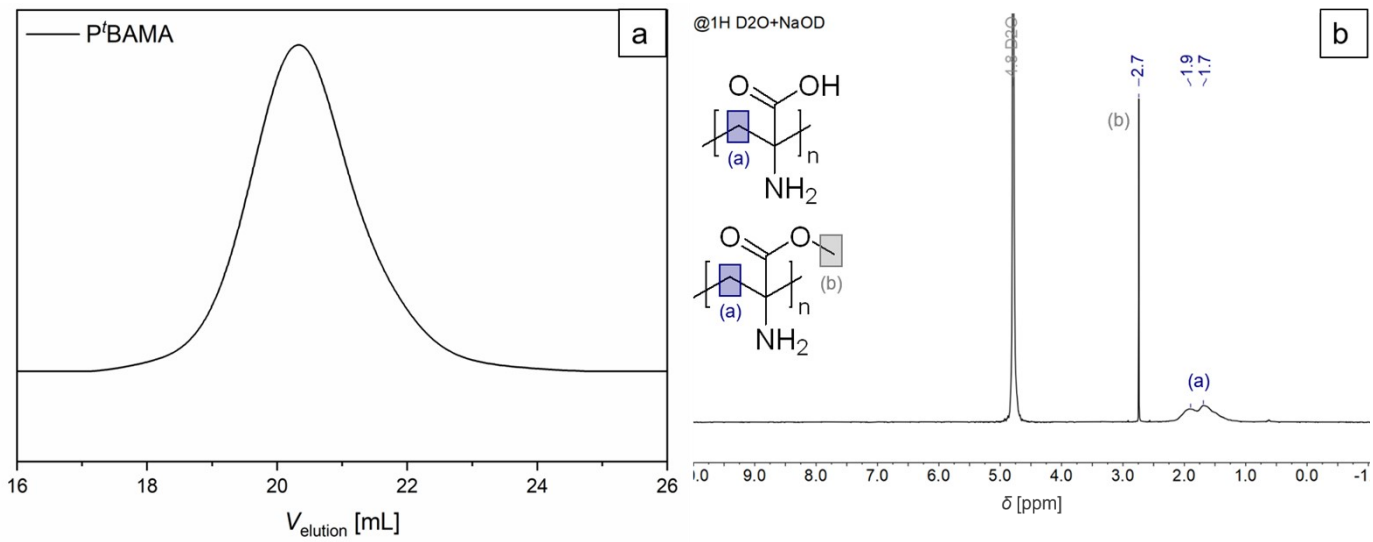

Figure S1: Analysis of the PDha macromonomer prior to use in gelation experiments: (a) SEC trace of pre-polymer P^{t}BAMA used for the synthesis of PDha in THF with M_n = 67000 g mol^{-1}, $Đ$ = 1.6 according to PMMA standard; (b) ^{1}H-NMR spectrum of PDha in D_2O/NaOD mixture (7:3). While the broad signal at 1.69 – 1.90 ppm indicates the protons in the R–CH_2–R group of PDha, the signal at 2.74 ppm refers to the –OMe group in carboxyl-protected PDha. Judging from the ratio of the signal integrals, ca. 15 % of the carboxyl functions in the original PDha polymer are esterified.

Reference:

1 U. Günther, L. V. Sigolaeva, D. V. Pergushov and F. H. Schacher, *Macromol. Chem. Phys.*, 2013, **214**, 2202–2212.

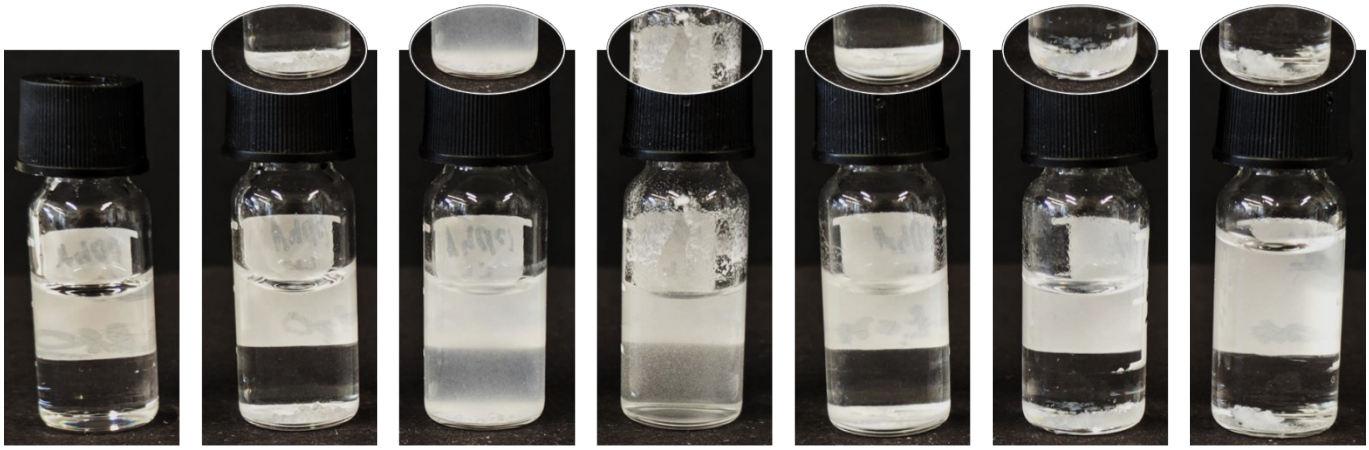

Figure S2: Experimental assessment of the solubility of PDha in various solvents by adding *m*(PDha) = 10 mg to *V*(solvent) = 1 mL and stirring the specimen for *t* = 1 week. As described in literature, only 0.1 M KOH and DMSO resulted in complete solvation of PDha. Even exposure to heat did not lead to sufficient solvation of PDha in the remaining solvents.

Rheological assessment of bulk hydrogels

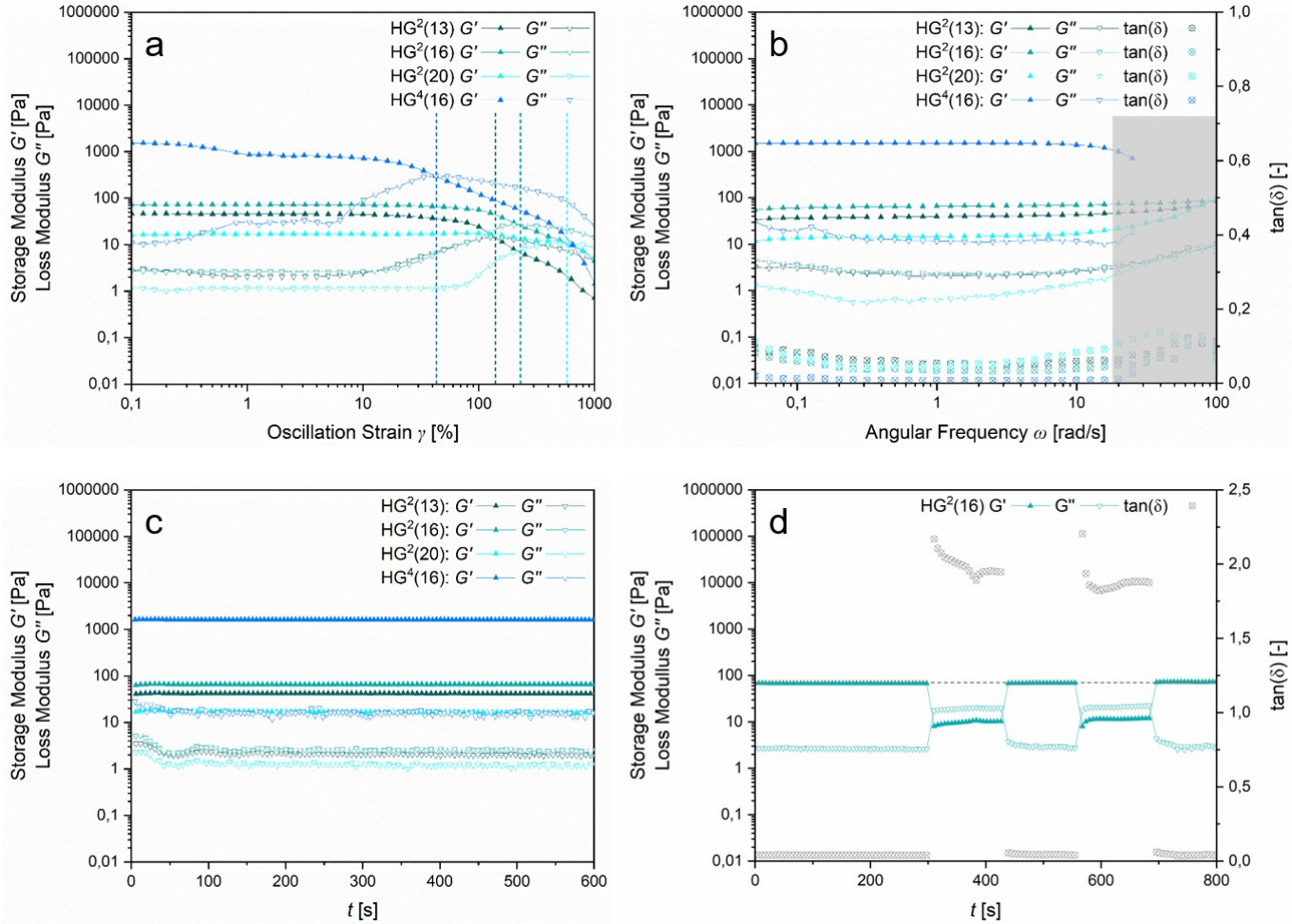

Figure S3: Rheology of hydrogels based on PEG-DGE and PDha. Storage modulus G' and loss modulus G'' were evaluated as a function of (a) oscillation strain γ ($\omega \approx 6.28$ rad/s for HG^2; $\omega \approx 3.14$ rad/s for HG^4), (b) angular frequency ω ($\gamma = 0.5$ % for HG^2; $\gamma = 0.2$ % for HG^4), and (c) time t ($\omega \approx 6.28$ rad/s and $\gamma = 0.5$ % for HG^2, $\omega \approx 3.14$ rad/s and $\gamma = 0.2$ % for HG^4). The grey bar in (b) indicates instrument limits. Repeated application of high strain ($\gamma = 500$ %, $\omega \approx 6.28$ rad/s) followed by relaxation at low strain ($\gamma = 0.5$ %, $\omega \approx 6.28$ rad/s) indicated self-regenerating behaviour of $HG^2(16)$ in (d).

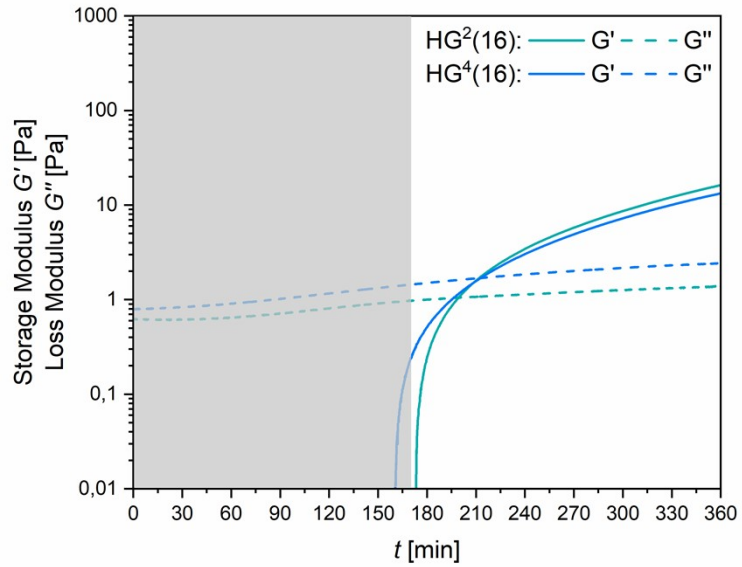

Figure S4: Rheological monitoring of the gelation between PEG-based crosslinker solution and PDha solution as prepared for $HG^2(16)$ and $HG^4(16)$. Storage modulus *G'* and loss modulus *G''* were measured as a function of time *t* ($\omega \approx 6.28$ rad/s and $\gamma = 0.5$ %). The grey bar indicates the limits of the rheometer.

Adaption of gelation for droplet-based microfluidic approach

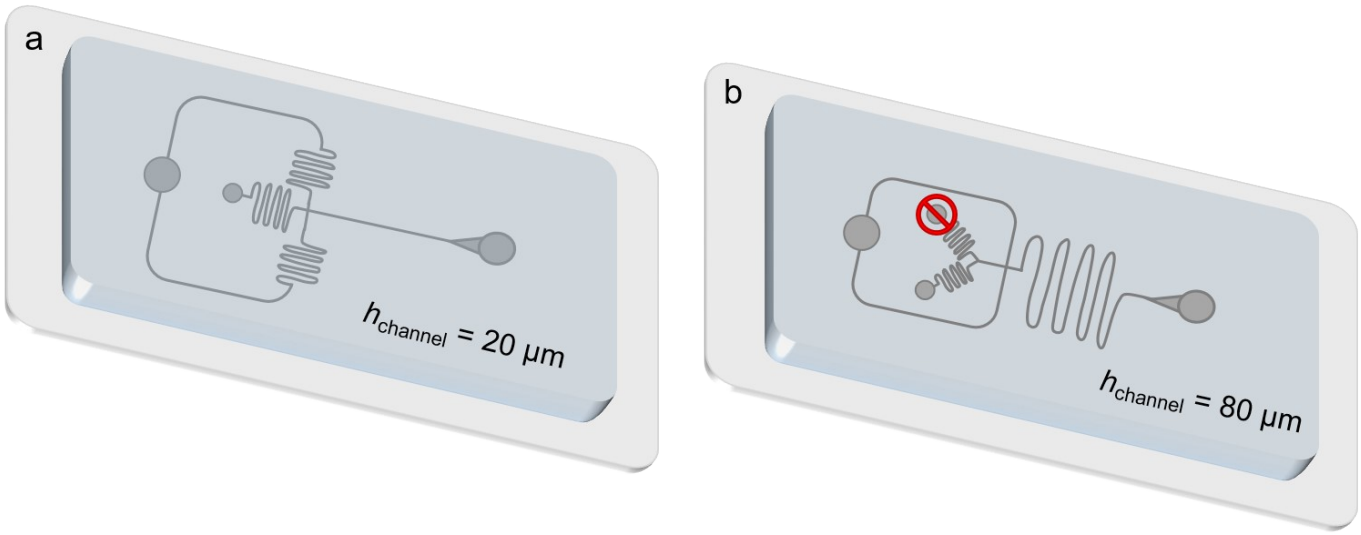

Figure S5: Schematic representation of the design of the PDMS-based microfluidic devices. The design (a) has a uniform height of 20 µm with one inlet for the continuous phase (left) and one inlet for the dispersed phase (middle). After formation of the droplets at the crossflow junction, the water-in-oil (w/o) emulsion runs straight to the outlet (right) as mixing of the reagent solutions is already ensured prior to their entry into the microfluidic channel. The design (b) has a uniform height of 80 µm with one inlet for the continuous phase (left) and two inlets for the dispersed phase (middle). After formation of the droplets at the crossflow junction, the w/o emulsion is led through a serpentine-shaped channel section to ensure thorough mixing. For the sake of simplicity, experiments with only one water phase were performed by not punching one of the respective inlets. In the chip design (b), we chose to omit the serpentine mixing section in the channel of the oil phase to reduce the risk of leakage.

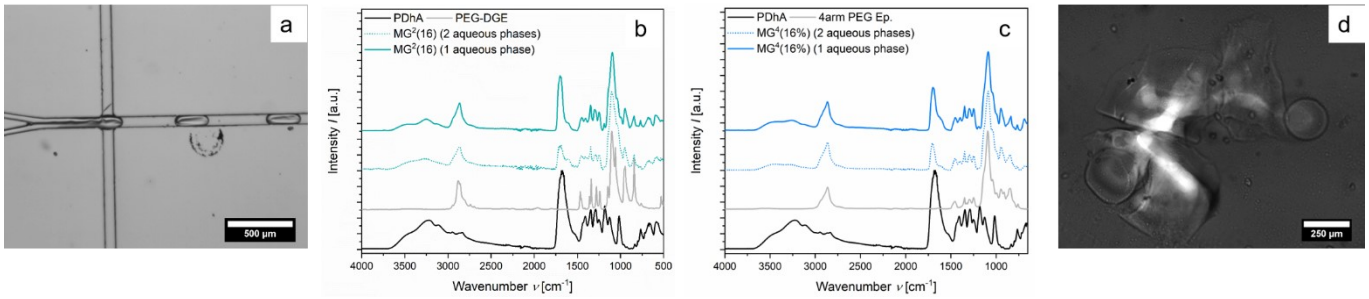

Figure S6: Illustration of the problems occurring when two separate aqueous phases of PEG-based crosslinker and PDha macromonomer, respectively, are used. Microscopic depiction of the mixture of the two phases at the crossflow junction in the microfluidic channel (a) shows that the two solutions maintain a clearly discernible interface. Even after mixing in the serpentine mixing section of the microfluidic channel, the solutions are not fully blended. The FTIR spectra of $MG^2(16)$ (b) and $MG^4(16)$ (c) demonstrate a significantly lower C=O vibration signal (1685 cm^{-1}) of the carboxylic acid groups within PDha when comparing with samples synthesized by use of one mixed aqueous phase. Imaging with optical microscopy (d) verifies that the gels fabricated with two aqueous phases are not stable and tear under mechanical stress (e.g. during purification).

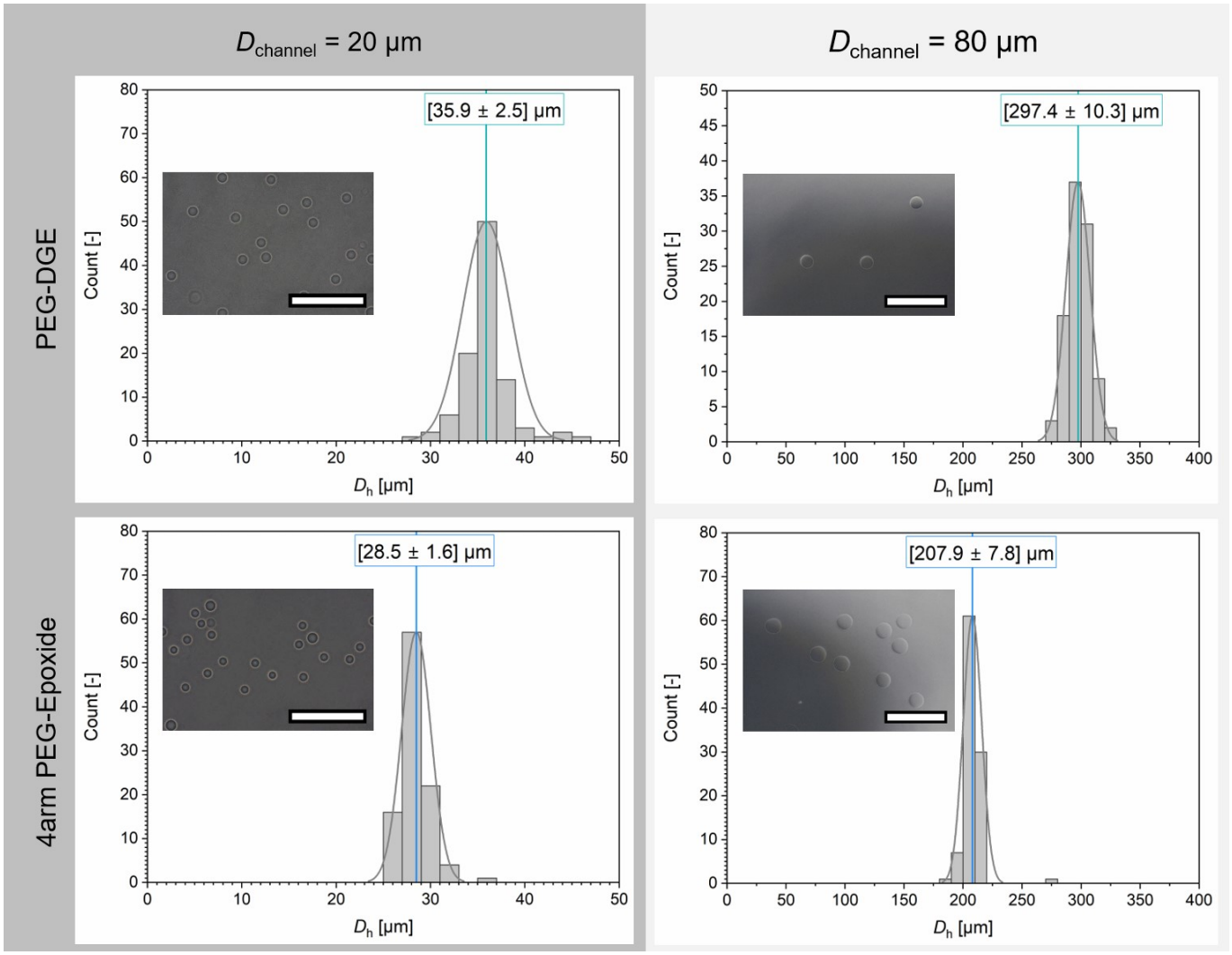

Figure S7: Morphology and size of the fabricated microgel species depending on the height of the microchannel and the type of crosslinker. The histograms were prepared by diluting the microgels in HPLC-grade water and recording images of the samples by optical microscopy before measuring the diameter of 100 microgels per sample. The vertical line indicates the mean hydrodynamic diameter of each sample. The inset images demonstrate optical microscopy images of the microgels (scale bars: 250 µm for the small microspheres, 1000 µm for the large microspheres). To improve the visibility of the microgels, a slit diaphragm was employed in the recording of these images.

Analysis of properties of the PDha-based microgels

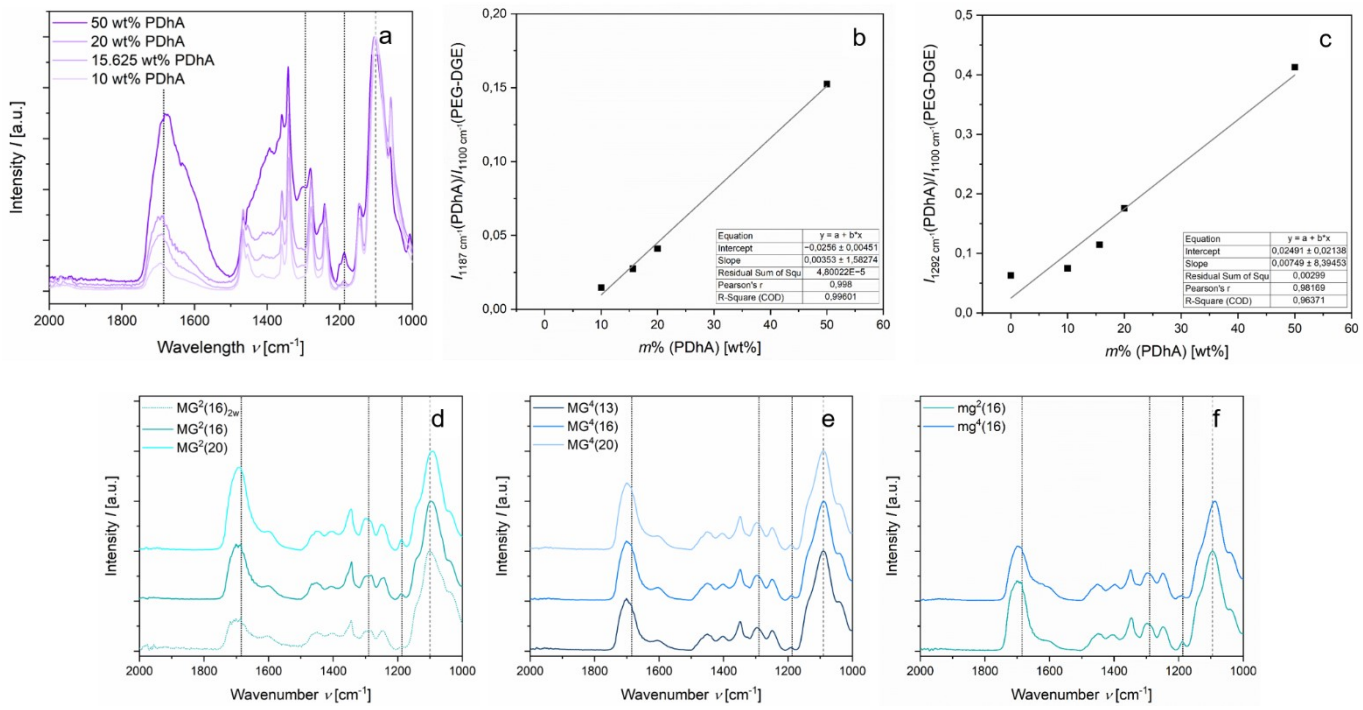

Figure S8: Depiction of the estimation of weight concentration *m*%(PDha) within the respective microgels. First, PDha and PEG-DGE were mixed so that aqueous solutions with a predefined weight concentration of PDha were obtained. The solutions were left to dry to obtain flakey solids. For each PDha concentration, three measurements were performed, then averaged and normalized (a). For the calibration curve, the C–O–C signal of PEG-DGE (1100 cm^{-1}) was considered and related to either the signal of C–N valence (1290 cm^{-1}) or the signal of C–N stretching (1187 cm^{-1}) within PDha. Though the signal of C=O valence (1685 cm^{-1}) is more intense, variations in the pH value during preparation of the calibration samples lead to shifting and broadening of the signal, corresponding to the deprotonation/protonation of the the carboxylic acid functions (a, d-f). The ratio of intensity between *I*(PDha) and *I*(PEG-DGE) was plotted as a function of the weight concentration of PDha and fitted linearly, once for *I*(PDha) = 1187 cm^{-1} (b) and once for *I*(PDha) = 1292 cm^{-1} (c). The ratio of the same signals was calculated from the sample curves (d-f) and then converted into the corresponding weight concentration using the linear equation.

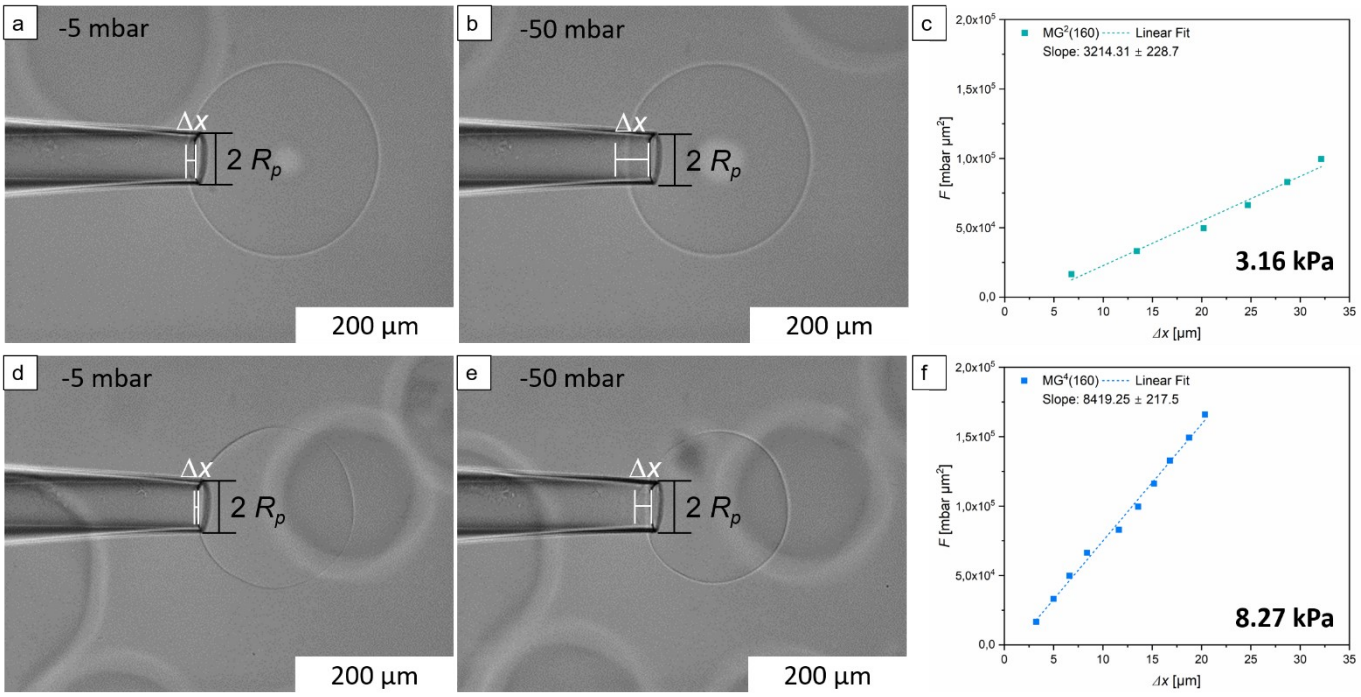

Figure S9: Brightfield microscopic images of the micropipette aspiration for $MG^2(16)$ (top) and $MG^4(16)$ (bottom), respectively, depicted at -5 mbar (a, d) and -50 mbar (b, e). Inset drawings show how the aspirated length Δx and the radius of the pipette R_p were determined from the images. The force F was plotted as a function of aspirated length Δx (c, f) and fitted linearily. The slope s of the linear fit function was then used in a simple continuum-medium model to calculate the effective Young's modulus (E, bold value in c and f).

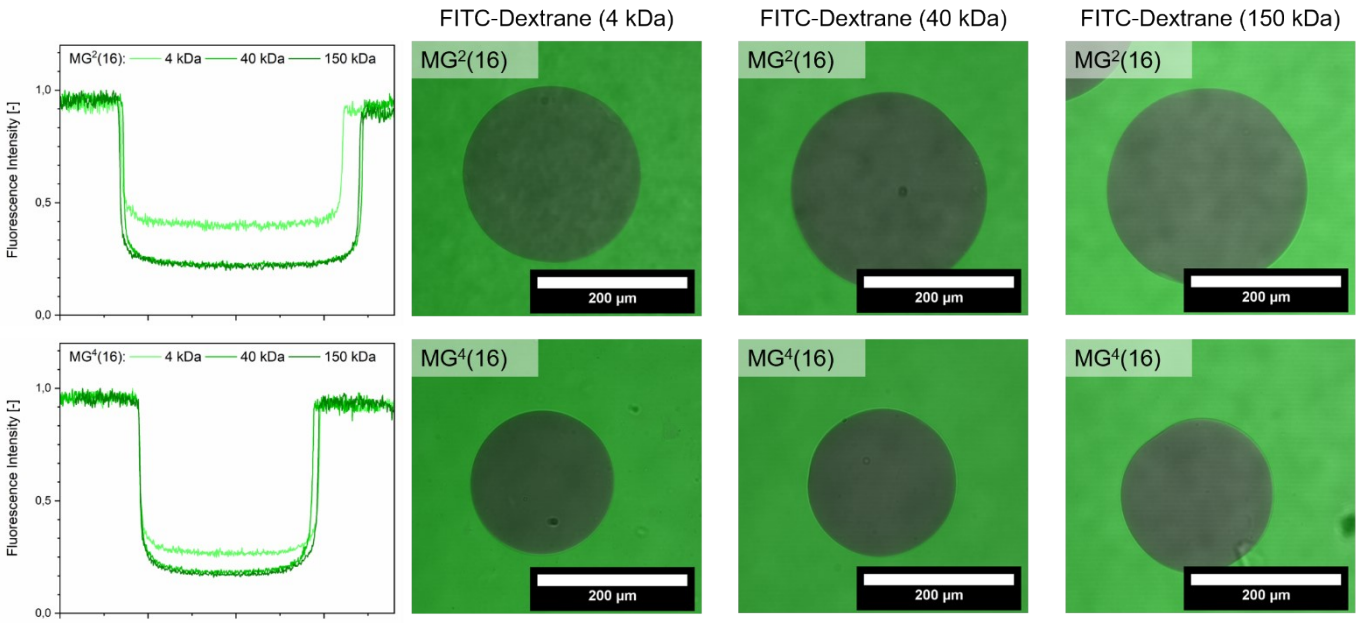

Figure S10: Fluorescence intensity profiles (left) determined by ROI analysis (region of interest) of the microgels dispersed in FITC-Dex. of different size. Corresponding CLSM fluorescence images of the microgel cross-sections are displayed (right).

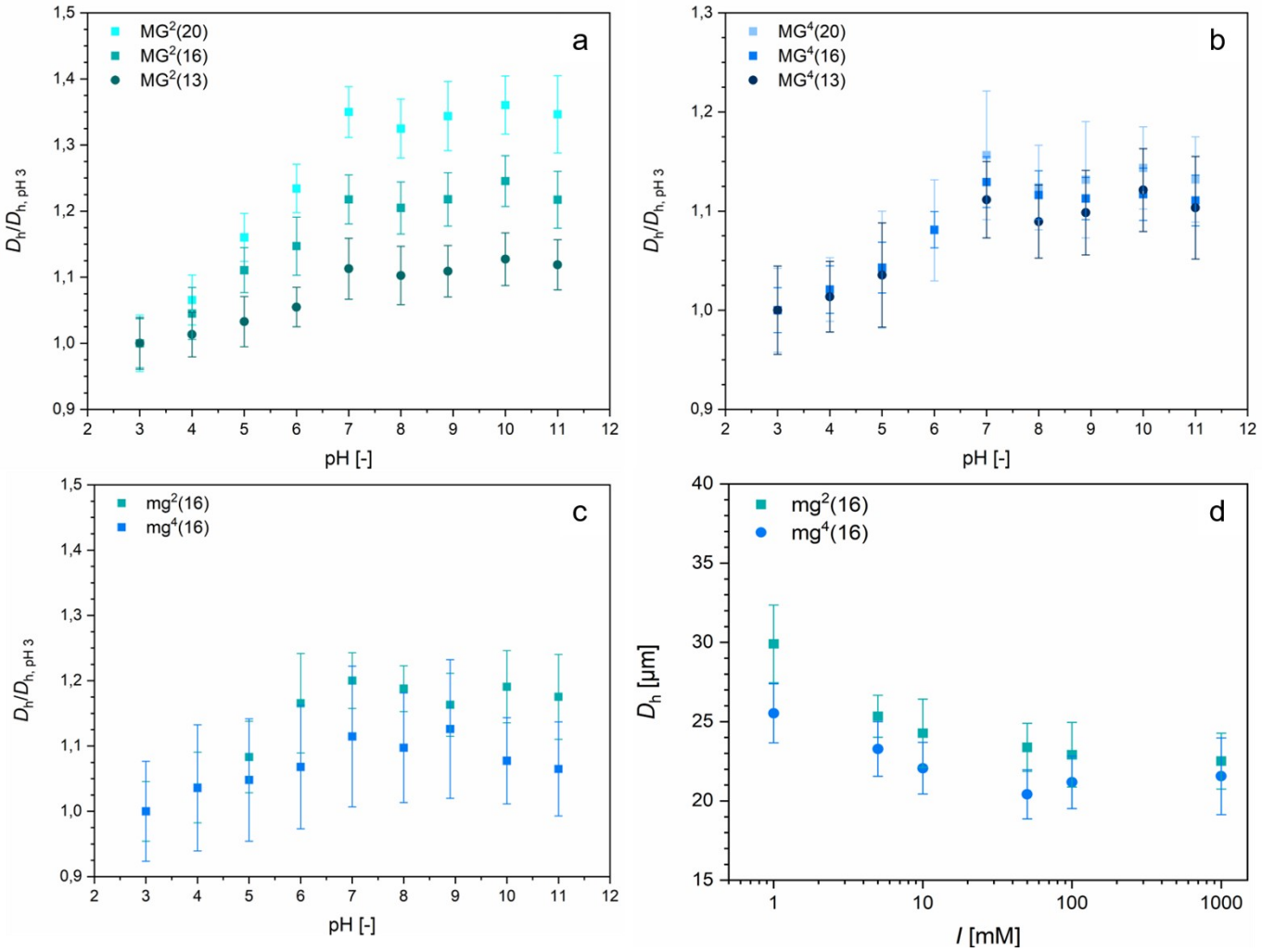

Figure S11: The pH-dependent swelling of various microgel samples is shown by plotting the swelling ratio $D_h/D_{h,pH3}$ against the pH-value of the buffer, in which the respective microgels are dispersed (a-c). Responsivity to ionic strength of the small microgels $mg^2(16)$ and $mg^4(16)$ is verified by presenting the hydrodynamic diameter D_h as a function of ionic strength *I*. All data points were gathered by measuring the diameter of 50 – 100 microgels per sample and averaging the values, with error bars indicating standard deviation.

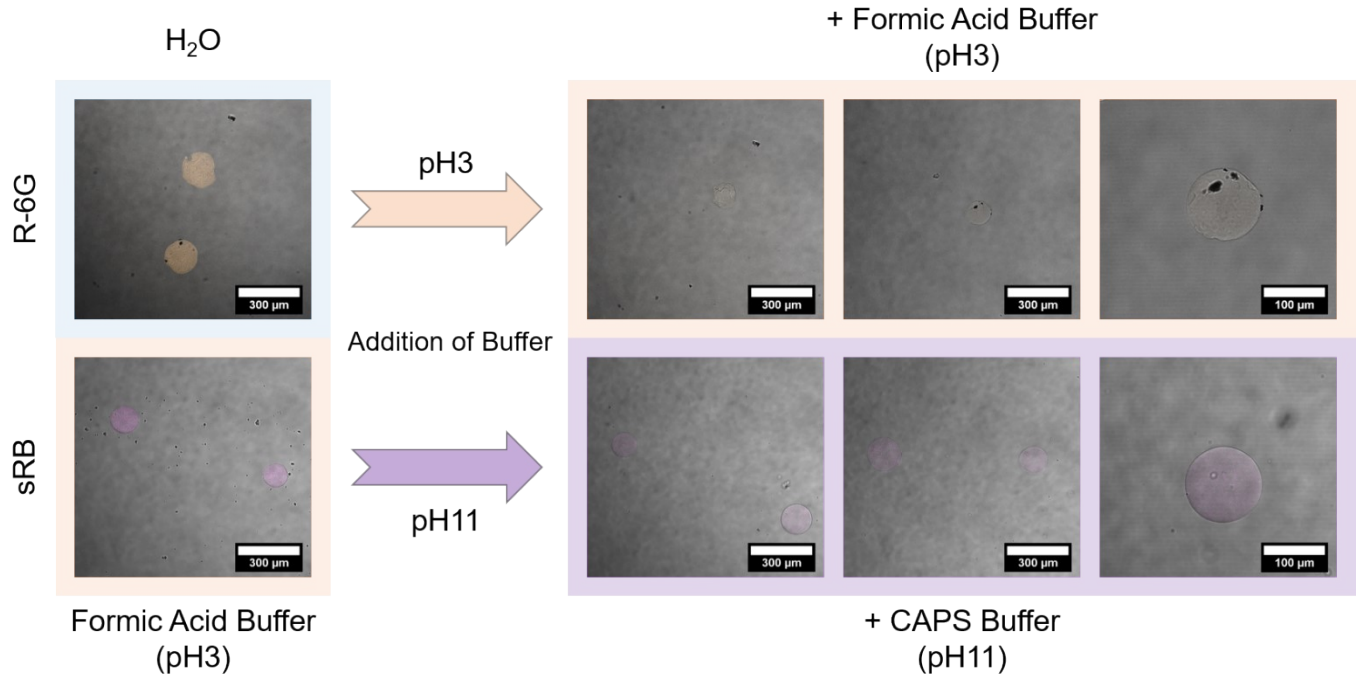

Figure S12: CLSM overlay images of pH-dependent release of charged model dyes R-6G (Ar laser: λ_{exc} = 514 nm at 10 %, *I* = 1 %, HyD with 50 % gain) and sRB (DPSS laser: λ_{exc} = 561 nm, *I* = 4 %, HyD with 400 % gain). To allow for comparison of fluorescence intensity, images belonging to the same microgel-dye sample were all measured using identical settings. Microgels loaded with R-6G in water immediately decolourized after the addition of formic acid buffer (top row). The change in pH-value and ionic strength led to a decrease in electrostatic attraction between the cationic dye and the microgels, since the carboxylate groups were either screened or protonated and the osmotic pressure changed. The desorption of sRB after addition of CAPS buffer to an acidic solution of sRB-containing microgels was significantly weaker (bottom row). On the one hand, there lack of change in ionic strength (salt concentration remained constant at *I* = 10 mM) could play a role; on the other hand, the resulting pH value is probably in the neutral rather than the basic range due to the mixing of formic acid buffer with CAPS buffer.

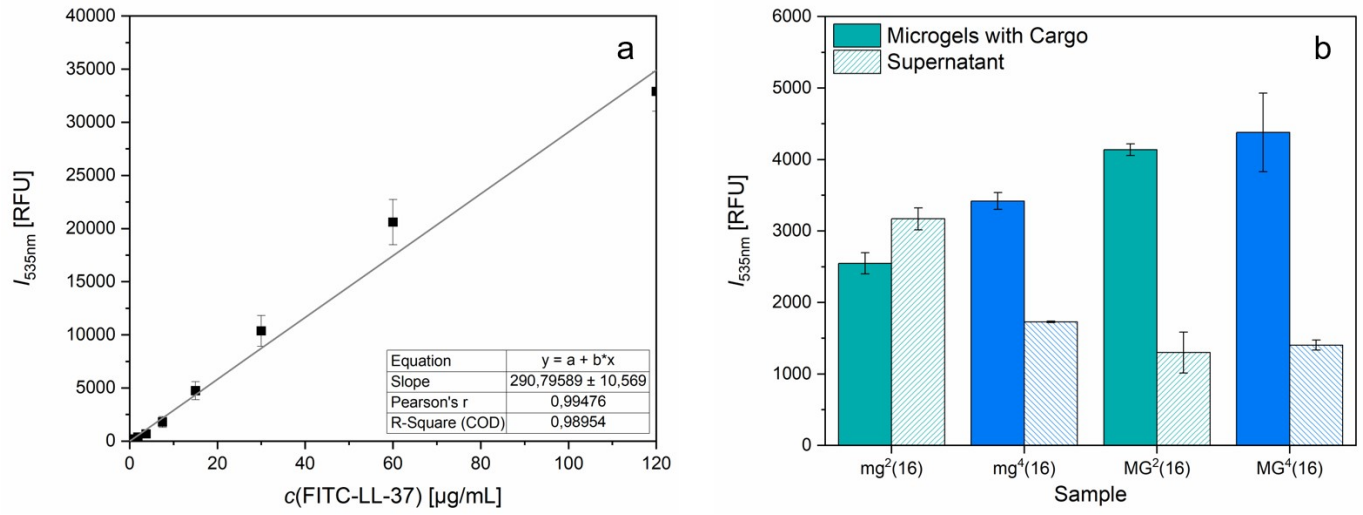

Figure S13: A calibration curve of the fluorescence intensity of FITC-LL-37 as a function of its concentration was determined by preparing corresponding aqueous FITC-LL-37 solutions by serial dilution and measuring the samples in a plate reader (a). The data points were fitted linearily. By employing the obtained linear function, the intensity signals of the samples and supernatants (b) could be converted into FITC-LL-37 concentrations. All intensity signals were measured in triplicate, with error bars displaying the standard deviation.